J. Braz. Chem. Soc., Vol. 22, No. 10, 1894-1902, 2011.
Printed in Brazil - ©2011 Sociedade Brasileira de Química
0103 - 5053 $6.00+0.00

Article

Effect of Cerium Loading on Structure and Morphology of Modified Ce-USY Zeolites

Fillipe A. C. Garcia,[a] Daniel R. Araújo,[a] Júnia C. M. Silva,[a] Julio L. de Macedo,[a] Grace F. Ghesti,[b] Sílvia C. L. Dias,*,[a] José A. Dias[a] and Geraldo N. R. Filho[c]

[a]Laboratório de Catálise, Instituto de Química and [b]Engenharia de Energia, Faculdade UnB-Gama, Universidade de Brasília, 70910-900 Brasília-DF, Brazil

[c]Centro de Ciências Exatas e Naturais, Universidade Federal do Pará, Rua Augusto Correa No. 1, 66075-010 Belém-PA, Brazil

Este trabalho descreve detalhadamente o efeito da quantidade de cério na estrutura e morfologia da zeólita NH_4USY. Ce-USY (2-25% m/m de CeO_2) foi obtido por impregnação úmida de $CeCl_3$ seguida de calcinação a 550 ºC por 8 h. Em quantidades baixas (2-10%), foi observado que as espécies de cério encontram-se nas posições de troca iônica na rede, enquanto em maiores teores (15-25%) pequenos agregados formaram-se na superfície da HUSY. Difratometria de raios X (XRD) mostrou apenas reflexões relacionadas à HUSY, confirmando a alta dispersão das espécies de cério, porém as análises por espectroscopia Raman com transformada de Fourier (FT-Raman) detectaram CeO_x para os materiais acima de 10%. A reação do $CeCl_3$ com NH_4USY produziu NH_4Cl, o qual se decompõe em HCl, ocasionando a desaluminização da rede. Os materiais apresentaram um aumento da razão Lewis/Brønsted com o aumento da quantidade de cério, devido a interação do excesso de cério com os grupos OH da USY e consequente formação de espécies CeO_x.

This work describes comprehensibly the effect of cerium loading on the structure and morphology of NH_4USY zeolite. The Ce-USY (2-25 wt.% of CeO_2) was obtained by wet impregnation of $CeCl_3$ followed by calcination at 550 ºC for 8 h. At low loadings (2-10%), cerium species are mainly located at ion exchange positions in the framework, whereas at higher loadings (15-25%), small aggregates were formed on the HUSY surface. X-ray diffractograms (XRD) exhibited only the reflections related to HUSY, demonstrating the high dispersion of cerium species, but Fourier transform Raman spectroscopy (FT-Raman) detected CeO_x for the materials above 10%. Reaction of $CeCl_3$ with NH_4USY produced NH_4Cl, which decomposed to form HCl, leading to framework dealumination. The materials showed an increased Lewis/Brønsted ratio with increasing cerium loadings due to the interaction between the excess cerium and the OH groups of USY, and the consequent formation of CeO_x species.

Keywords: cerium USY zeolite, cerium oxide, ultra stable Y zeolite, solid-state ion exchange, ^{27}Al and ^{29}Si MAS NMR spectroscopy

Introduction

Faujasite-type zeolites (X and Y) are largely applied in fluid catalytic cracking (FCC) of crude oil distillates and in hydrodesulfurization of fossil diesel oil and gasoline.[1] Y zeolites, either in their sodium or ammonium form, can be exchanged for rare earth ions to achieve the following main goals: (*i*) to prevent aluminum loss from the zeolite structure, which results in enhanced structural resistance to the severe hydrothermal conditions of the regeneration step of FCC,[2] and (*ii*) to increase the activity, because the introduction of rare earth species modifies the number of acidic protons through either hydrolysis or enhancement of ionic fields inside the zeolite structure.[3] Because rare earth cations modify the acidic properties of zeolites, their insertion has an effect on both thermal and mechanical stability, which are important for zeolite application to industrial processes such as pyrolysis,[4] oxidation,[5,6] cracking,[2] hydrogenation,[7] alkylation[8,9] and the Fries rearrangement.[10]

*e-mail: scdias@unb.br, jdias@unb.br

The use of ceria-based catalysts has been well established for a variety of environmental applications, such as oxidation of diesel soot,[10] hydrodesulfurization of fossil diesel oil,[1] low temperature naphthalene and CO oxidation,[11-13] H_2S adsorption,[14] water gas shift process[15] and construction of hydrogen fuel cells.[16] These applications, especially the oxidation processes, are related to oxygen storage capacity (OSC), which reflects the ability of ceria to release oxygen upon reduction of Ce^{IV} and to adsorb oxygen upon the oxidation of Ce^{III}, completing a redox cycle and allowing the *in situ* regeneration of the catalyst by gas flow.[17]

The incorporation of cerium species into zeolites has resulted in materials that combine the high activity of ceria with the high surface area and selectivity of zeolites. Reddy *et al.*[18] demonstrated the application of cerium(III)-modified zeolites (*e.g.*, HZSM-5, MOR and HY) to the photogeneration of hydrogen from water. Velu *et al.*[19] reported that the addition of Ce^{IV} species to Y zeolites increased sulfur adsorption capacity and selectivity in comparison with aromatics in jet fuel. These results have indicated that removal of thiophene is greatly influenced by cerium oxidation number and content, the amount of adsorbed water and the structure of the zeolite framework.

Although several studies on cerium-modified zeolites exist, the relationship between cerium loading and zeolite structure is uncertain and has not been systematically approached with respect to the changes that zeolites undergo upon the addition of different amounts of cerium. Therefore, the goal of this work was to synthesize and characterize Ce-USY catalysts within a wide loading range (2-25 wt.% of CeO_2) to study the effect of cerium oxide content on both the structure and morphology of USY.

Experimental

Synthesis of Ce-USY zeolites

Ce-USY catalysts of 2, 5, 10, 15 and 25 wt.% were prepared by aqueous impregnation. Cerium chloride heptahydrate ($CeCl_3 \cdot 7H_2O$, Vetec, 99.9%) was used as Ce^{III} source and a USY zeolite in the ammoniacal form (Zeolyst, CBV500, SiO_2/Al_2O_3 = 5.2, Na_2O = 0.2%) was used as support. The metal and the support were added to a 100 mL round-bottom flask with an adequate amount of water to obtain a 1:10 (catalyst:water) mass ratio. Each slurry sample was stirred at 80 ºC until all water evaporated. Finally, the solid was calcined at 550 ºC for 8 h in a EDG muffle furnace (model 3P-S) with a heating rate of 10 ºC min^{-1} to obtain the total decomposition of the cerium precursor and the protonic form of the zeolite. After calcination, the catalysts were characterized by a number of techniques, employing the experimental conditions described as follows.

Characterization of Ce-USY zeolites

Thermogravimetric/derivative thermogravimetric/differential thermal analyses (TGA/DTG/DTA) data were obtained in a simultaneous TGA/DTA/DSC equipment (model SDT 2960, TA Instruments) with a heating rate of 10 ºC min^{-1} from room temperature (*ca.* 25 ºC) up to 800 ºC under a synthetic air (99.999%) flow of 50 mL min^{-1}. Platinum pans loaded with about 15 mg of sample were used in all runs with α-Al_2O_3 as reference.

Nitrogen adsorption/desorption isotherms were obtained at −196.15 ºC using a gas adsorption analyzer (model Nova 1200, Quantachrome). Surface area and pore volume data were obtained through BET and BJH adsorption and desorption isotherms, respectively. Before analysis, each sample was degassed for 1 h under vacuum conditions (10^{-5} mm of Hg) at 300 ºC.

Gas phase pyridine (py) adsorption was conducted simultaneously for all samples. Platinum crucibles loaded with the samples (20 mg) were placed in a shallow porcelain plate and inserted into a glass reactor adapted to a tubular furnace (model F21135, Thermolyne). The catalysts were dehydrated in dried N_2 (100 mL min^{-1}) at 300 ºC for 1 h and cooled to 100 ºC, and then gaseous pyridine diluted in N_2 was allowed to pass through the samples for 1 h. The temperature was held at 150 ºC under N_2 for 2 h to remove physically adsorbed pyridine. Subsequently, the samples were analyzed by Fourier transform infrared spectroscopy (FTIR).

X-ray fluorescence (XRF) spectra were obtained with a Shimadzu EDX 720 spectrophotometer with a rhodium X-ray source tube. The XRF spectra were collected under vacuum conditions (< 45 Pa) using two channels, with the X-ray source set at 50 and 15 kV for Ti-U and Na-Sc, respectively. The cerium elemental composition of the prepared samples was determined through an analytical curve built with CeO_2 pellets diluted with H_3BO_3. The silicon and aluminum content were determined by comparison with fundamental standards (Quali-Quant method).

X-ray powder diffraction (XRD) patterns were recorded on a Bruker D8 FOCUS diffractometer operating at 40 kV and 30 mA with Cu-K_α radiation (λ = 1.5418 Å) and a graphite monochromator. The Bragg angle (2θ) range was scanned from 2 to 40º at 2 degrees min^{-1}. Before the experiment, each sample was mixed with 15 wt.% of elemental Si as an internal standard. This standard allows the normalization of the position and intensity of

the diffractogram, so that the Bragg angle and intensity values can be used to calculate the crystallinity (ASTM D 3906-80) and the unit cell parameter a_0 (ASTM D3942-80), according to the literature.[20]

Infrared (FTIR) spectra were recorded on a Nicolet 6700 spectrophotometer (Thermo Scientific) with 128 scans and a spectral resolution of 4 cm^{-1}. Each sample was pressed into dried KBr (1 wt.%, Merck) pellets. Framework Si/Al ratios were calculated by equation 1:[21]

$$x = 3.857 - 0.00621\ w_{DR}\ (cm^{-1}) \quad (1)$$

where $0.1 < x < 0.3$, w_{DR} is the zeolite specific double ring vibration mode between 570 and 600 cm^{-1} and $x = [1 + (Si/Al)]^{-1}$.

Fourier transform Raman (FT-Raman) spectra were obtained at room temperature (*ca.* 25 ºC) with 256 scans and a resolution of 4 cm^{-1} on a spectrophotometer Bruker (FRA 106/S module attached to an Equinox 55). The wavelength and laser (Nd-YAG) power were 1064 nm and 100 mW, respectively. A liquid N_2-cooled Ge detector collected the Raman signal.

Solid state nuclear magnetic resonance (MAS NMR) experiments were performed with a Varian Mercury Plus spectrometer (7.05 T) equipped with a 7 mm probe (zirconia rotors with torlon caps). ^{29}Si spectra (59.609 MHz) were recorded with magic angle spinning (MAS) at a speed of 3 kHz, a single pulse duration of 5.5 μs (π/2), a recycle delay of 20 s and 500 scans. ^{27}Al spectra (78.188 MHz) were recorded with MAS at a speed of 6 kHz, a single pulse duration of 1.0 μs (π/18), a recycle delay of 0.4 s and 2000 scans. The ^{29}Si and ^{27}Al spectra were referenced to the external standards tetramethylsilane and $[Al(H_2O)_6]^{3+}$, respectively (δ = 0 ppm). MAS NMR spectra were deconvoluted using a Gaussian mathematical fit.

Scanning electron (SEM) micrographs were obtained with a Zeiss microscope (LEO 1430) operating at 10 kV and 90 mA of beam current. The samples were metalized and supported on carbon tape. All micrographs were obtained under vacuum.

Results and Discussion

Elemental analysis (XRF)

Elemental analysis of the cerium catalysts and of the pure USY zeolite were performed using X-ray fluorescence (XRF) and energy-dispersive X-ray spectroscopy (EDS) measurements to evaluate the actual amount of cerium (reported as CeO_2) on each catalyst, the elemental composition of the zeolite and the presence of possible contaminants (*e.g.*, NaCl). The results for the USY zeolite identified the presence of Si and Al, and, together with the TGA/DTG data (described in the next section), allowed the determination of both water and ammonium contents to obtain the following chemical formula of the zeolite: $(NH_4^+)_{39.7}(H_2O)_{169.5}[Al_{39.7}Si_{152.3}O_{384}]$-USY.

In addition, the results for the supported catalysts indicated that the cerium oxide loadings were in close agreement with the nominal values, and the preparation error did not exceed ± 10% of each value (Table 1). Thus, the nominal values will be used henceforth for simplicity. The differences between the nominal and the measured values are probably due to the water content in the cerium chloride precursor. In addition, no chloride was observed in the materials after calcination, which revealed that the precursor was completely decomposed as also attested by TGA (see next section).

Thermal evolution and textural characterization

Before calcination, DTG curves of the Ce-USY materials presented two mass losses at approximately 110 and 350 ºC (Figure 1). They are related to desorption of water molecules that were physically/chemically adsorbed onto the zeolite surface, followed by evolution of NH_3 and HCl. These gases were produced from the decomposition of the NH_4^+ counter ion combined with Cl^- from the $CeCl_3$ precursor. In addition, the temperature of the NH_4^+ decomposition shifted from 400 ºC for the pure zeolite (Figure 1a) to *ca.* 370 ºC for the exchanged materials.

Table 1. Elemental analysis and textural characterization results of HUSY and Ce-USY catalysts containing 2-25 wt.% CeO_2 calcined at 550 ºC for 8 h

Sample[a]	CeO_2 / wt.%	S_{BET} / ($m^2\ g^{-1}$)	S_{Micro} / ($m^2\ g^{-1}$)	Pore volume / ($cm^3\ g^{-1}$)
0[b]	–	780	731	0.03
2	2.1	574	552	0.02
5	5.4	589	563	0.02
10	11.5	577	538	0.03
15	14.5	495	470	0.02
25	23.9	406	389	0.02

[a]Nominal CeO_2 loadings (wt.%) on USY zeolite; [b]HUSY calcined at 550 ºC for 8 h.

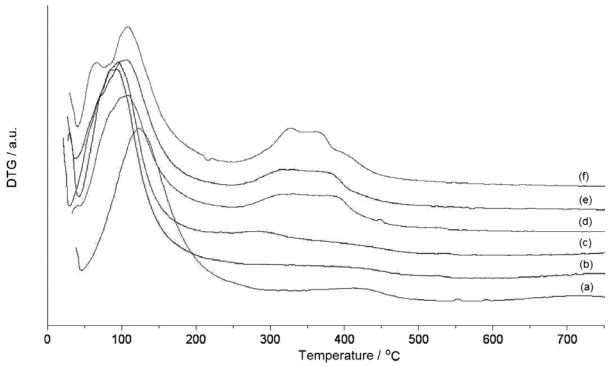

Figure 1. DTG curves, all before calcination, of HUSY (a) and Ce-USY catalysts containing 2 (b), 5 (c), 10 (d), 15 (e) and 25 wt.% of CeO_2 (f).

Actually, the substitution of NH_4^+ ions for Ce^{3+} may have resulted in formation of NH_4Cl due to the presence of Cl^- ions, which remained in the solid after impregnation. Pure NH_4Cl salt usually decomposes by sublimation at about 350 ºC; however, this temperature may change due to the confinement of NH_4Cl inside the pores of the zeolite.[20] In contrast, TGA curves obtained after calcination at 550 ºC for 8 h exhibited only the first mass loss (Figure S1), which is evidence of complete decomposition of the metal precursor, the ammonium counter ion and/or ammonium chloride during calcination. Furthermore, the TGA curve of the NH_4USY zeolite presented a 20% mass loss, which is related to water desorption and was used to determine the 169.5 H_2O molecules in the chemical formula presented earlier.

Adsorption and desorption of nitrogen in HUSY and Ce-USY zeolites (Figure S2) exhibited reversible type II isotherms (IUPAC classification) that posed an initial increase in the P/P_0 values up to 0.2-0.3, characteristic of nitrogen adsorption on the zeolite micropores, followed by an exponential increase related to adsorption on multiple superposed layers.[22-25] Similar nitrogen adsorption isotherms were reported by Yao *et al.*[26] and Schneider *et al.*[27] for sodalite and NaY zeolites, respectively.

The zeolite desorption isotherms were analyzed using BET and BJH methods to obtain specific surface areas and pore volumes, respectively (Table 1). The Ce-USY zeolites may be gathered in two different sample sets including one with low Ce loading (2-10 wt.%) and another with high cerium loadings (15 and 25 wt.%). The samples with low loadings presented specific surface areas of around 580 $m^2\ g^{-1}$, while those with higher oxide contents exhibited surface areas of around 495 and 406 $m^2\ g^{-1}$ for 15 and 25 wt.%, respectively. This decrease in surface area was because cerium species can be deposited on the inner pores and/or on the external surface of the support. Cerium species that are not at ion exchange positions interact with surface sites (*e.g.*, silanol groups) to facilitate particle aggregation with further grain agglomeration, which could lead to formation of CeO_x with lower surface areas. The pore volumes did not change considerably among the samples, suggesting a good dispersion of cerium particles on the surface of the support. Finally, t-plot analysis of the adsorption isotherms (Table 1) revealed that the microporosity of the materials decreased as the content of cerium increased, indicating that the cerium species were preferentially located inside the cavities.

X-ray diffraction analysis

The diffractograms of the Ce-USY catalysts exhibited only the reflections given by the USY zeolite and elemental silicon ($2\theta = 28.45^o$) added as internal standard. No peaks related to the fluorite structure of CeO_2 (2θ = 28.6, 33.3 and 47.5º) were found.[28] These results indicated that Ce^{IV} species were well dispersed on the support surface[29,30] even at loadings as high as 25 wt.% (Figure 2), which was in agreement with the nitrogen adsorption-desorption data. In addition, a decrease in the relative intensity of the peaks related to the support with increased cerium loading was observed. This finding was attributed to the loss in zeolite crystallinity and to the higher cerium absorption coefficient of X-ray radiation.[2,31]

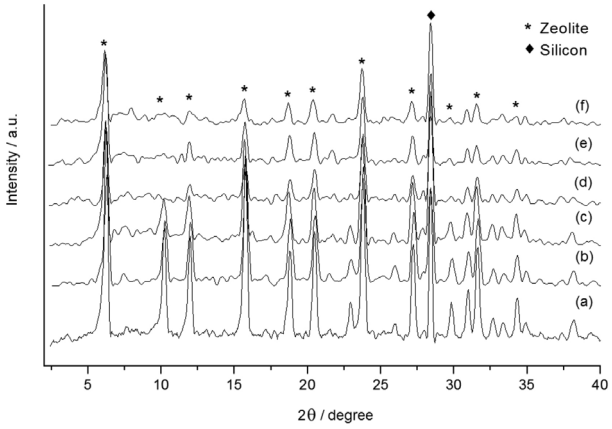

Figure 2. Diffractograms of HUSY (a) and Ce-USY catalysts calcined at 550 ºC for 8 h containing 2 (b), 5 (c), 10 (d), 15 (e) and 25 wt.% of CeO_2 (f).

The ASTM D 3906-80 method allowed the quantitative evaluation of the crystallinity parameter using peak intensities at 2θ = 10.2, 11.9, 15.7, 18.8, 20.5, 23.8, 27.2, 30.9, 31.6 and 34.3º, which are related to the reflections on the [220], [311], [331], [511] and [333], [440], [533], [642], [660] and [822], [555] and [751] and [664] planes, respectively. It is important to note that the reflections at the [220] and [311] planes were not originally included in the ASTM method, but were included here to obtain

a more accurate crystallinity value.[20] This parameter for Ce-USY catalysts presented a reduction with increasing cerium loadings.

The unit cell parameters (a_0) were calculated using ASTM method D3942-80 after normalization of the diffractograms using an elemental Si standard. The unit cell contracts with an increase of dealuminization and with a decreased amount of TO_4 tetrahedra.[32,33]

The a_0 values of Ce-USY zeolites depend on structural factors that include the dealuminization process, the ion exchange extent and the presence and location of extra-framework aluminum and cerium species. The range of a_0 values (24.48-24.60 Å) obtained for Ce-USY samples (Table 2) was associated with the balance between the dealumination process and the migration of cerium species upon calcination to positions inside the sodalite cage.[34,35] According to Nery *et al.*,[33] cerium exchange species are located inside supercages and migrate to sodalite cage sites during calcination, which increases the value of a_0. However, the calcination process of zeolites is usually accompanied by framework dealumination that decreases a_0, as well as the presence of hydrated rare-earth species and the decomposition of NH_4Cl, which produces protons that catalyze aluminum hydrolysis.[34,35] The occurrence of these two processes simultaneously explains the gradual loss of crystallinity of the samples with cerium loading, although full interpretation of the unit cell parameters from XRD is very difficult.

Table 2. XRD crystallinity and Si/Al ratio results for Ce-USY zeolites containing 2-25 wt.% of CeO_2 calcinated at 550 ºC for 8 h

Sample[a]	Crystallinity / %	$(Si/Al)_{FTIR}$	a_0 / Å
0[b]	100	4.5	24.52
2	73.1	4.9	24.48
5	59.7	5.4	24.57
10	27.7	7.0	24.53
15	28.0	7.0	24.55
25	19.9	7.9	24.60

[a]Nominal CeO_2 loading (wt.%) on USY support; [b]HUSY calcined at 550 ºC for 8 h.

Fourier transform infrared and Raman spectroscopies

The FTIR spectra of Ce-USY zeolites before calcination presented bands at 1630, 1400, 1180, 1050, 818, 590, 510 and 450 cm^{-1} (Figure S3). The bands at 1630 and 1400 cm^{-1} are related to the bending vibrations of O–H and N–H groups from adsorbed water and NH_4^+ counter ions, respectively. In addition, the bands at 1180 and 818 cm^{-1} are associated with external linkages among TO_4 tetrahedra (T = Si, Al), which are surface-sensitive, while those at 1050 and 450 cm^{-1} are related to internal linkages of TO_4 tetrahedra, which are related to the bulk of USY zeolite.[36] Because the band at 590 cm^{-1}, which is associated with the zeolite specific double ring vibration mode, is very sensitive to changes in zeolite structure, it was used to calculate the framework Si/Al ratio for all samples.[20,37] The results obtained (Table 2) showed that, before calcination, the framework Si/Al ratio of the samples remained the same as in the parent material (around 4.0).

After calcination, the samples presented lower intensity in all structural bands of the USY zeolite and the band at 1400 cm^{-1} disappeared (Figure 3). These results corroborate the loss of crystallinity obtained from XRD. In addition, the decomposition of NH_4Cl led to the formation of HCl that catalyzed aluminum hydrolysis, increasing the framework dealumination process and the framework Si/Al ratio with cerium loading, which reached a value of 7.9 (Table 2).

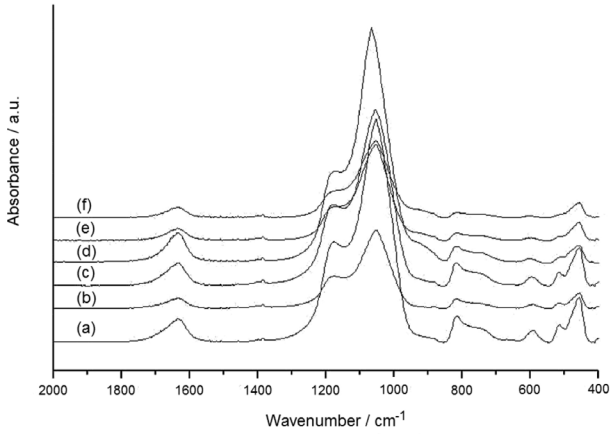

Figure 3. FTIR spectra of HUSY (a) and Ce-USY catalysts calcined at 550 ºC for 8 h containing 2 (b), 5 (c), 10 (d), 15 (e) and 25% wt.% of CeO_2 (f).

The FT-Raman spectra of the Ce-USY zeolites are presented in Figure 4. The materials with low loadings (0-10 wt.%) showed only one band at 500 cm^{-1} related to the USY zeolite.[38] Nonetheless, the materials with 15 and 25 wt.% cerium exhibited an intense Raman shift at 465 cm^{-1}. This band is associated with the symmetric breathing mode of oxygen at neighboring positions of the Ce^{IV} ion and is characteristic of a fluorite structure (*Fm*3*m* space group).[39-41] The absence of this band for materials with loadings lower than 10 wt.% and its appearance in materials with 15 wt.% is related to the higher degree of the NH_4^+-Ce^{3+} ion exchange process. The expected limit of exchange was 13 wt.%, so that the excess cerium in non-exchangeable sites have formed small CeO_x species responsible for the observed Raman shift. This result is consistent with nitrogen adsorption and XRD data, since

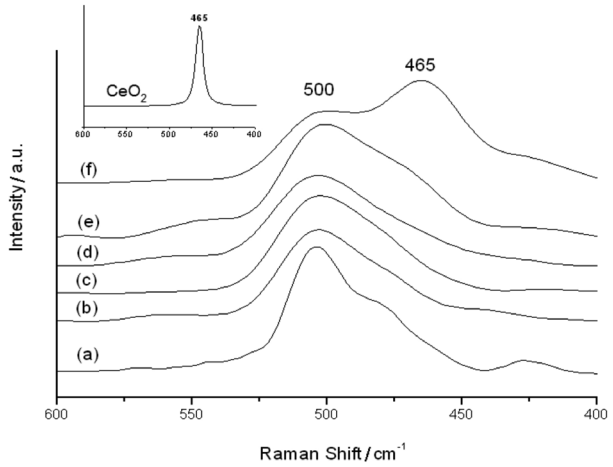

Figure 4. FT-Raman spectra of HUSY (a) and Ce-USY catalysts containing: 2 (b), 5 (c), 10 (d), 15 (e) and 25% wt.% of CeO_2 (f) calcined at 550 ºC for 8 h. The spectrum of CeO_2 (inset) is also shown for comparison.

small crystallites of CeO_2 did not show any peak in the diffractograms of the materials.

Solid-state nuclear magnetic resonance spectroscopy

The ^{29}Si MAS NMR spectra of HUSY and Ce-USY containing 2-25 wt.% are shown in Figure S4. Ce-USY zeolites displayed five silicon environments (even after deconvolution) that were differentiated by the number of aluminum atoms on the second coordination sphere: Si(3Al), Si(2Al), Si(1Al), Si(0Al) and extra-framework silicon species. These sites appear at −89.2, −96.6, −101.3, −106.4 and −110 ppm respectively.[20,32,42] The relative intensities of these signals after deconvolution are shown in Table S1. The signal related to the Si(4Al) environment was not observed in the NMR spectra because the ultrastabilization process removed a considerable amount of framework aluminum,[43] which eliminated the presence of this type of environment. In addition, the increasing contribution of extra-framework silicon species with cerium loading indicated that SiO_4 tetrahedra were removed from the zeolitic structure. The observed increase of the Q^4 silicon environment was related to the polymerization of monomeric extra-framework silicon species because the Si(0Al) environment of the samples was practically constant. Lutz *et al.*[32] showed that acid treatment of a dealuminated zeolite led to the formation of polymeric SiO_2 species within the structure of the zeolite, assigned at approximately −110 ppm in the NMR spectrum (silica gel Q^4 environment). As already discussed, the procedure used to prepare Ce-USY zeolites was accompanied by the formation of NH_4Cl, which decomposed forming HCl that catalyzes silicon polymerization. Although the SiO_2 Q^4 environment could be identified, the presence of other non-framework phases (*e.g.*, silica gel Q^2 and Q^3 environments, monomeric SiO_2) cannot be completely excluded due to limitations of the spectral deconvolution method.

The ^{27}Al MAS NMR spectra of HUSY and Ce-USY zeolites containing 2-25 wt.% presented two peaks at −0.4 and 59.1 ppm related to octahedral, *i.e.*, Al(VI), and tetrahedral, *i.e.*, Al(IV) sites, respectively (Figure 5). In addition, a decrease in the intensity of the Al(VI) peak with increasing CeO_2 loading was observed due to the loss of crystallinity, as determined by XRD results. Ghesti *et al.*[22] reported a decrease in the intensity of EFAL and Si−O(H)−Al groups at 3642 and 3566 cm^{-1} using diffuse reflectance infrared Fourier transform spectroscopy (DRIFTS). There was also a convoluted signal between −0.4 and 59.1 ppm, which might be related to the presence of aluminum in distorted octahedral and/or tetrahedral sites.[43,44]

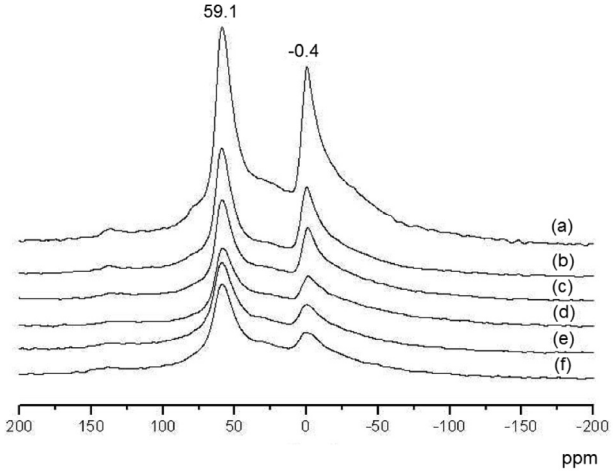

Figure 5. ^{27}Al MAS NMR spectra of HUSY (a) and Ce-USY catalysts calcined at 550 ºC for 8 h containing 2 (b), 5 (c), 10 (d), 15 (e) and 25% wt.% of CeO_2 (f).

The distribution of tetrahedral, octahedral and convoluted signals (intermediate aluminum sites) allowed a better comprehension of the dealumination process that the USY zeolite underwent upon calcination (Figure 6). The dealumination process involves the transformation of Al atoms from the structure to extra-framework atoms. Decreased tetrahedral sites and increased octahedral sites were observed with increasing cerium loadings up to 10 wt.%. The samples with higher loadings (15 and 25 wt.%) showed HCl concentrations that were capable of completely removing some of the Al(IV) sites from the zeolite framework, which decreased the intermediary species and increased the amount of octahedral sites.[20]

Scanning electron microscopy

SEM micrographs of HUSY and Ce-USY catalysts are shown in Figure 7. HUSY presented smooth spherical

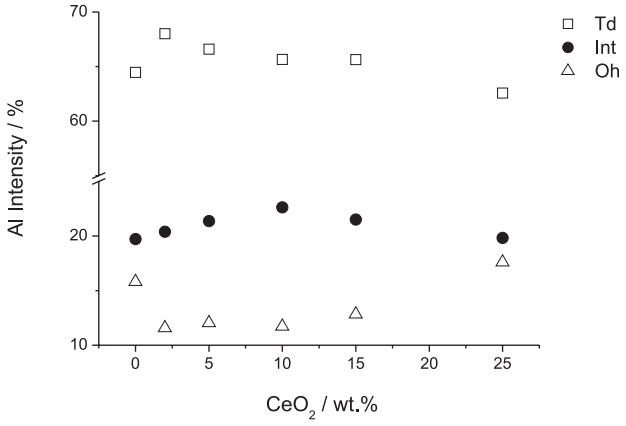

Figure 6. Plot of the distribution of tetrahedral (Td), octahedral (Oh) and intermediate (Int) aluminum sites of the Ce-USY catalysts (all calcined at 550 ºC for 8 h) as a function of cerium loading.

particles of *ca.* 500 nm of diameter with a homogeneous distribution throughout the solid. The catalysts with 2-10 wt.% presented no perceptible morphological changes in comparison to HUSY, while those with 15 and 25 wt.% exhibited agglomerates that increased in number and in diameter up to 4 μm. This remarkable difference between the samples with low oxide loading and those with 15 and 25 wt.% is related to a much higher sinterization of cerium species in these samples.

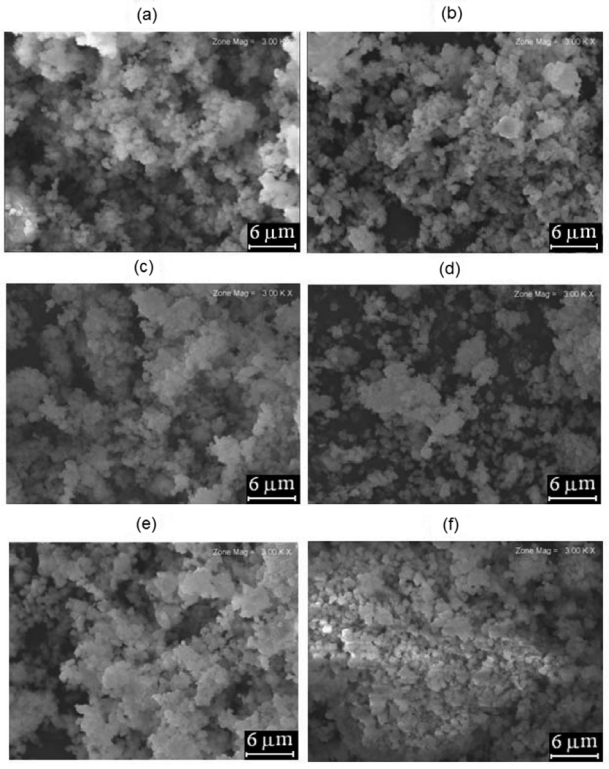

Figure 7. SEM micrographs of HUSY (a) and Ce-USY catalysts calcined at 550 ºC for 8 h containing 2 (b), 5 (c), 10 (d), 15 (e) and 25% wt.% of CeO_2 (f).

Ce-USY acidity

The Ce-USY acidity was investigated with gas phase adsorption of pyridine to correlate with the overall surface acidity of the samples. Pyridine was used to probe the acidity of Ce-USY samples by FTIR (Figure 8), which identified Brønsted and Lewis sites.[44,45] The spectra showed three bands at 1545, 1490 and 1445 cm^{-1}, which are associated to Brønsted sites, a combination of Brønsted/Lewis sites and Lewis sites respectively.[46-48] The acidity of cerium materials has been widely discussed, but there is no consensus about the types of acid sites present on their surfaces.[49,50] Gu *et al.*[49] reported the presence of Brønsted and Lewis sites in CeO_2 by ammonia adsorption studies. Ghesti *et al.*[22] reported recently two types of acid sites with enthalpies of −117.6 kJ mol^{-1} and −83.6 kJ mol^{-1}, which were assigned to Brønsted, and a combination of weak Brønsted/Lewis sites for 5 wt.% Ce-HUSY. The impregnation of cerium reduced the acidity of the HUSY zeolite, which previously had Brønsted sites with enthalpies of −134.0 kJ mol^{-1} and −101.5 kJ mol^{-1}, through the interaction with Si−O(H)−Al bridges, as observed by DRIFTS measurements. Although a definitive assignment of the hydroxyl bands in USY zeolites cannot be performed at this moment, the bands at 3566 and 3642 cm^{-1} were more affected by cerium than the other ones, indicating that the ion exchange between cerium ions and protons occurred during impregnation steps.[22]

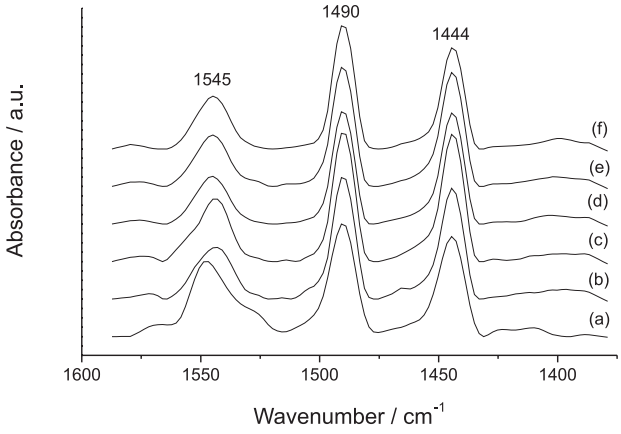

Figure 8. FTIR spectra of HUSY and Ce-USY (calcined at 550 ºC for 8 h) after pyridine adsorption and thermal desorption at 150 ºC: HUSY (a) and Ce-USY catalysts containing 2 (b), 5 (c), 10 (d), 15 (e) and 25% wt.% of CeO_2 (f).

In the present study, an increase of the Lewis/Brønsted ratio with increasing cerium loadings was observed (Table 3), which was attributed to a decrease of Brønsted sites that interacted with cerium species and an increase of Lewis sites. For the samples with 15 and 25% loadings, a

Table 3. Ratios between the Lewis and Brønsted sites obtained from the FTIR spectra after gaseous pyridine adsorption followed by thermal desorption at 150 ºC

Sample[a]	(L_{py}/B_{py})[b] ratio
0	0.92
2	1.44
5	1.45
10	1.69
15	1.60
25	1.37

[a]Nominal CeO_2 loading (wt.%) on USY support (HUSY calcined at 550 ºC for 8 h); [b]L_{Py} and B_{Py}: pyridine interacting with Lewis and Brønsted sites, respectively.

decrease of the ratio could be an indication of the formation of cerium agglomerates with 25% loading, as observed with both SEM micrographs and FT-Raman spectroscopy.

Conclusions

The analysis of Ce-USY catalysts prepared with a wide loading range (2-25 wt.% of CeO_2) was performed with reliable techniques that provided valuable information regarding structural and morphological changes that USY underwent depending on cerium content.

Characterization of Ce-USY materials indicated that the samples with low cerium loadings (2-10%) exhibited ion exchange degrees below the stoichiometric threshold, which led to the formation of Ce^{IV} species linked to negatively charged Al in the framework. In addition, the samples with high loadings (15-25%) exceeded this threshold, so that CeO_x species were formed on the zeolite surface. The X-ray diffractograms of the Ce-USY catalysts exhibited only the reflections related to USY zeolite, demonstrating either interaction with USY or high dispersion of cerium species. Zeolite structural changes were also studied and are related to HCl formation by NH_4Cl decomposition. The higher amount of HCl generated with higher cerium loadings led to an increase in the Q^4 silicon environment, which is related to the polymerization of monomeric extra-framework silicon species. The high amount of HCl is also associated with a gradual extraction of the Al(IV) sites from the zeolite framework, forming distorted tetrahedra and/or octahedra for higher cerium concentrations (15-25%).

The acidity of Ce-USY materials was also affected by cerium loading. The FTIR spectra showed the presence of both Brønsted and Lewis acidic sites. An increase in the Lewis/Brønsted ratio with increasing cerium loadings was observed and attributed to the interaction of zeolite OH surface groups with cerium species as well as an increase of Lewis sites with excess cerium. For the samples with 15 and 25% loading, the decrease of the ratio was consistent with the formation of CeO_x agglomerates, as observed in the SEM micrographs and detected by FT-Raman spectra.

Supplementary Information

Supplementary data (Figures S1-S4 and Table S1) are available free of charge at http://jbcs.org.br as a PDF file.

Acknowledgments

We thank the Conselho Nacional de Desenvolvimento Científico e Tecnológico (CNPq) for research, doctorate and undergraduate scholarships and acknowledge the financial support given by UnB/DPP/IQ, Coordenação de Aperfeiçoamento de Pessoal de Nível Superior (CAPES), Fundação de Empreendimentos Científicos e Tecnológicos (FINATEC), Financiadora de Estudos e Projetos (FINEP/CTPetro, FINEP/CTInfra), Fundação de Apoio à Pesquisa do Distrito Federal (FAPDF) and Ministério da Ciência e Tecnologia (MCT/CNPq).

References

1. Xue, M.; Chitrakar, R.; Sakane, K.; Hirotsu, T.; Ooi, K.; Yoshimura, Y.; Toba, M.; Fengb, Q.; *J. Colloid Interface Sci.* **2006**, *298*, 535.
2. Puente, G.; Aguiar, E. F. S.; Zontin, F. M. Z.; Camorim, V. L. D.; *Appl. Catal., A* **2000**, *197*, 41.
3. Souza-Aguiar, E. F.; Camorin, V. L. D.; Zotin, F. M. Z.; Santos, R. L. C.; *Microporous Mesoporous Mater.* **1998**, *25*, 25.
4. Boxiong, S.; Chunfei, W.; Cai, L.; Binbin, G.; Rui, W.; *J. Anal. Appl. Pyrolysis* **2007**, *78*, 243.
5. Atoguchi, T.; Kanougi, T.; Yamamoto, T.; Yao, S.; *J. Mol. Catal. A: Chem.* **2004**, *220*, 183.
6. Neamtu, M.; Catrinescu, C.; Kettrup, A.; *Appl. Catal., B* **2004**, *51*, 149.
7. Zheng, J.; Guo, M.; Song, C.; *Fuel Process. Technol.* **2008**, *89*, 467.
8. Salinas, A. L. M.; Sapaly, G.; Taarit, Y. B.; Vedrine, J. C; Essayem, N.; *Appl. Catal., A* **2008**, *336*, 61.
9. Al-Khattaf, S.; Rabiu, S.; Tukur, N. M.; Alnaizy, R.; *Chem. Eng. J. (Amsterdam, Neth.)* **2008**, *139*, 622.
10. Sartori, G.; Maggi, R.; *Chem. Rev. (Washington, DC, U. S.)* **2006**, *106*, 1077.
11. Garcia, T.; Solsona, B.; Taylor, S. H.; *Appl. Catal., B* **2006**, *66*, 92.
12. Zhang, D.; Pan, C.; Shi, L.; Huang, L.; Fang, J.; Fu, H.; *Microporous Mesoporous Mater.* **2009**, *117*, 193.

13. Beck, A.; Horváth, A.; Stefler, G.; Katona, R. O.; Geszti, G.; Tolnai, L. F.; Liotta, L.; Guczi, A.; *Catal. Today* **2008**, *139*, 180.
14. Petre, C. F.; Larachi, F.; *Ind. Eng. Chem. Res.* **2005**, *44*, 9391.
15. Gasser-Ramirez, J. L.; Dunn, B. C.; Ramirez, D. W.; Turpin, G. C.; Shi, Y.; Ernst, R. D.; Pugmire, R. J.; Eyring, E. M.; Pettigrew, K. A.; Rolison, D. R.; Harris, J. M.; *J. Non-Cryst. Solids* **2008**, *354*, 5509.
16. Yeung, C. M. Y.; Yu, K. M. K.; Fu, Q. J.; Thompsett, D.; Petch, M. I.; Tsang, S. C.; *J. Am. Chem. Soc.* **2005**, *127*, 18010.
17. Di Monte, R.; Fornasiero, P.; Graziani, M.; Kaspar, J.; *J. Alloys Compd.* **1998**, *275*, 877.
18. Reddy, J. K.; Suresh, G.; Hymavathi, C. H.; Kumari, V. D.; Subrahmanyam, M.; *Catal. Today* **2009**, *141*, 89.
19. Velu, S.; Ma, X.; Song, C.; *Ind. Eng. Chem. Res.* **2003**, *42*, 5293.
20. Giannetto, G.; *Zeolitas: Características, Propriedades y Aplicaciones Industriales*; Editorial Innovación Tecnológica: Caracas, Venezuela, 1990.
21. Lutz, W.; Rüscher, C. H.; Heidemann, D.; *Microporous Mesoporous Mater.* **2002**, *55*, 193.
22. Ghesti, G. F.; Macedo, J. L.; Parente, V. C. I.; Dias, J. A.; Dias, S. C. L.; *Microporous Mesoporous Mater.* **2007**, *100*, 27.
23. Galwey, A. K.; Brown, M. E.; *Studies in Physical and Theoretical Chemistry*, vol. 86; Elsevier: Amsterdam, 1999.
24. Figueiredo, J. L.; Ribeiro, F. R.; *Catálise Heterogênea*; Fundação Calouste Gulbenkian: Lisboa, Portugal, 1989.
25. Adamson, A. W.; Gast, A. P.; *Physical Chemistry of Surfaces*, 6th ed.; John Wiley & Sons: New York, 1997.
26. Yao, J.; Zhang, L.; Wang, H.; *Mater. Lett.* **2008**, *62*, 4028.
27. Schneider, P.; Hudec, P.; Solcova, O.; *Microporous Mesoporous Mater.* **2008**, *115*, 491.
28. Damyanova, S.; Perez, C. A.; Schmal, M.; Bueno, J. M. C.; *Appl. Catal., A* **2002**, *234*, 271.
29. Weckhuysen, B. M.; Schoonheydt, R. A.; *Catal. Today* **1999**, *49*, 441.
30. Garcia, F. A. C.; Silva, J. C. M.; Macedo, J. L.; Dias, J. A.; Dias, S. C. L.; Filho, G. N. R.; *Microporous Mesoporous Mater.* **2008**, *113*, 562.
31. Rauscher, M.; Kesore, K.; Mönnig, R.; Schwieger, W.; Tibler, A.; Turek, T.; *Appl. Catal., A* **1999**, *184*, 249.
32. Lutz, W.; Toufar, H.; Heidemann, D.; Salman, N.; Rüscher, C. H.; Gesing, T. M.; Buhl, J.; Bertram, R.; *Microporous Mesoporous Mater.* **2007**, *104*, 171.
33. Nery, J. G.; Mascarenhas, Y. P.; Bonagamba, T. J.; Mello, N. C.; Sousa-Aguiar, E. F.; *Zeolites* **1998**, *18*, 44.
34. Lee, E. F. T.; Rees, L. V. C.; *Zeolites* **1987**, *7*, 446.
35. Lee, E. F. T.; Rees, L. V. C.; *Zeolites* **1987**, *7*, 143.
36. El-Bahy, Z. M.; *Mater. Res. Bull.* **2007**, *42*, 2170.
37. Moreira, C. R.; Schmal, M.; Pereira, M. M.; *Stud. Surf. Sci. Catal.* **2000**, *143*, 915.
38. Li, J.; Xiong, G.; Feng, Z.; Liu, Z.; Xin, Q.; Li, C.; *Microporous Mesoporous Mater.* **2000**, *39*, 275.
39. Smith, E.; Dent, G.; *Modern Raman Spectroscopy: A Practical Approach*; Wiley: New York, 2005.
40. Krishna, K.; Bueno-López, A.; Makkee, M.; Moulijn, J. A.; *Appl. Catal., B* **2007**, *75*, 189.
41. Al-Yassir, N.; Le Van Mao, R.; *Appl. Catal., A* **2007**, *332*, 273.
42. Gore, K. U.; Abraham, A.; Hedge, S. G.; Kumar, R.; Amoureux, J.; Ganapathy, S.; *J. Phys. Chem. B* **2002**, *106*, 6115.
43. Engelhardt, G.; Michel, D.; *High-Resolution Solid-State NMR of Silicates and Zeolites*; John Wiley & Sons: New York, 1987.
44. Chronister, C. W.; Drago, R. S.; *J. Am. Chem. Soc.* **1993**, *115*, 4793.
45. Drago, R. S.; Dias, S. C.; Torrealba, M.; Lima, L.; *J. Am. Chem. Soc.* **1997**, *119*, 4444.
46. Kanellopoulos, J.; Unger, A.; Schwieger, W.; Freude, D.; *J. Catal.* **2006**, *237*, 416.
47. Garcia, F. A. C.; Braga, V. S.; Silva, J. C. M.; Dias, J. A.; Dias, S. C. L.; Davo, J. L. B.; *Catal. Lett.* **2007**, *119*, 101.
48. Zaki, M. I.; Hasan, M. A.; Al-Sagheer, F. A.; Pasupulety, L.; *Colloids Surf., A* **2001**, *190*, 261.
49. Gu, X.; Ge, J.; Zhang, H.; Auroux, A.; Shen, J.; *Thermochim. Acta* **2006**, *451*, 84.
50. Watanabe, M.; Osada, M.; Inomata, H.; Arai, K.; Kruse, A.; *Appl. Catal., A* **2003**, 245, 333.

Submitted: February 21, 2011
Published online: July 26, 2011